The effect of hydrogen bonding on diffusion and permeability in UV-cured Polyacrylate-based networks for controlled release

AUTHOR(S)

Bing Wu, Walter Chassé, Klaus Zick, Michael D Mantle, Andreas Heise, Dermot F Brougham, Victor M Litvinov

Journal of Controlled Release 327 (2020) 150–160

Contents lists available at ScienceDirect

Journal of Controlled Release

journal homepage: www.elsevier.com/locate/jconrel

The effect of hydrogen bonding on diffusion and permeability in UV-cured Polyacrylate-based networks for controlled release

Bing Wu[a,b,c,**], Walter Chassé[d], Klaus Zick[e], Michael D. Mantle[f], Andreas Heise[c], Dermot F. Brougham[b,*], Victor M. Litvinov[g,*]

[a] National Institute for Cellular Biotechnology, School of Chemical Sciences, Dublin City University, Glasnevin, Dublin 9, Ireland
[b] School of Chemistry, University College Dublin, Belfield, Dublin 4, Ireland
[c] Department of Chemistry, Royal College of Surgeons in Ireland, 123 St. Stephen's Green, Dublin 2, Ireland
[d] Institut für Physikalishe Chemie, Universtiy of Münster, Corrensstr. 28/30, 48149 Münster. Germany
[e] Bruker Biospin GmbH, Silberstreifen 4, 76287 Rheinstetten, Germany
[f] Department of Chemical Engineering and Biotechnology, University of Cambridge, Pembroke Street, Cambridge, UK
[g] V. Lit Consult, Gozewijnstraat 4, 6191WV, Beek, the Netherlands

ARTICLE INFO

Keywords:
Hydrogen bonding
Coating
Pulsed-field gradient NMR
NMR relaxometry
DSC thermoporometry
Molecular self-diffusion

ABSTRACT

Polyacrylates are important polymers widely used in pharmaceutical industry such as drug coatings due to their low cost, processability and ease of functionalisation. Chemical functionalities (*e.g.* H-bonding) can be easily included to modulate the transport of low molecular weight drug-like entities through the network. Understanding how such microscopic structural modifications determine macroscopic diffusion is critical for designing next generation responsive polymers. In this study pulsed field gradient (PFG) ^{1}H NMR measurements of the self-diffusion of a dye molecule (Eosin Y) in a series of polyacrylate networks with differing H-bonding strength were undertaken; it was found that the diffusion of Eosin Y is significantly reduced in networks with H-bonding. Detailed analyses by ^{1}H NMR relaxometry and double quantum (DQ) NMR show that H-bonding can also reduce polymer chain mobility. Furthermore, DSC thermoporometry showed a significant increase in the average network mesh size potentially due to the pre-organization of H-bonding containing monomer during network curing. By introducing the H-bonding disrupter, $LiClO_4$, it was found that the diffusivity of solute becomes positively correlated to the average mesh size across the series of networks. Hence, a modified diffusion model based on hydrodynamic theory is proposed to separate the direct (solute-network) H-bonding contribution to solute diffusion from the indirect contribution arising from monomer pre-ordering induced mesh size reduction. Finally, it is shown that the same direct and indirect contributions to microscopic diffusivity, arising from the H-bond strength of the co-monomers, also contribute significantly to the macroscopic membrane permeability which is similarly subject to H-bond disruption.

1. Introduction

Polymer coatings which have the ability to encapsulate therapeutic reagents have played an important role in developing controlled drug delivery systems (CDDSs) [1,2]. Several natural and synthetic macromolecules have been successfully used for formulating coatings and different types of drug release behaviors have been observed [3,4]. Over the past two decades considerable work has been done to improve the performance of polymeric drug coatings [5,6]; hence drug release profiles, tailored to a given pharmacological treatment, have been pursued by optimising CDDS formulation and processing parameters (coating thickness, type of loading additives *etc.*) [7–9]. However, more detailed understanding of how these, and other physico-chemical factors, determine local diffusion properties, is required for designing improved CDDSs.

Among all the polymeric drug coatings, polyacrylic networks are the most widely used in commercial production due to their proven biocompatibility and ease of manufacture on an industrial scale by UV-induced photo-curing. However, UV-cured networks are often heterogeneous on the molecular scale due to the complex kinetics of photo-initiated radical polymerization [10]. Poorly controlled kinetics can also complicate the optimisation of processing parameters for obtaining

* Corresponding author.
** Corresponding author at: Department of Chemistry, Royal College of Surgeons in Ireland, 123 St. Stephen's Green, Dublin 2, Ireland
E-mail addresses: bingwu@rcsi.ie (B. Wu), dermot.brougham@ucd.ie (D.F. Brougham).

https://doi.org/10.1016/j.jconrel.2020.07.039
Received 5 March 2020; Received in revised form 21 July 2020; Accepted 22 July 2020
Available online 30 July 2020

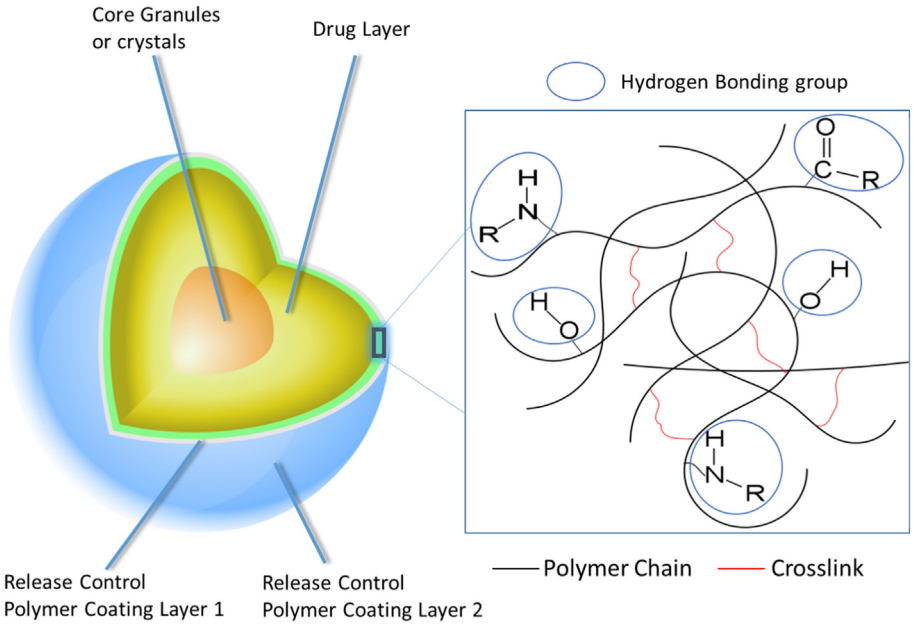

Fig. 1. A typical CDDS polymer coating. Hydrogen bonding groups are used to tailor the diffusion property of the polymer coating layer.

Table 1
Details of chemicals used for network formation.

Compounds	Structure	M_w (g/mol)
Hexyl acrylate (HA)	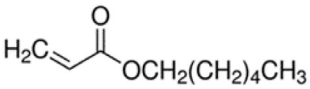	156.22
Poly(ethylene glycol) diacrylate (PEGDA)	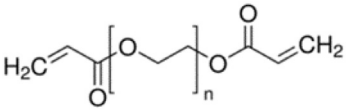	700
4-Hydroxybutyl acrylate (HBA)	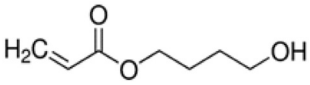	144.17
2-[[(Butylamino)carbonyl]oxy]ethyl acrylate (BAC)	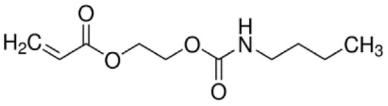	215.5
2,2-Dimethoxy-2-phenylacetophenone	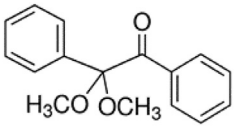	256.3
Eosin Y disodium salt	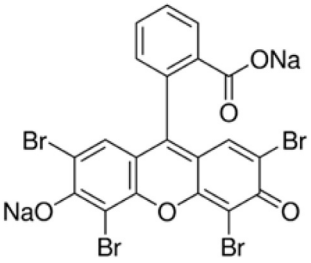	691.85

uniform coatings with desired diffusion properties. One common way to modulate diffusivity is by including additional chemical moieties, *e.g.* hydrogen bonding groups, into the pre-polymerization monomer formula, as suggested in Fig. 1, which can alter the interactions between the pharmaceutics and the resulting polymer network [11], and perhaps also the kinetics of polymerization. Hence it is of great interest to study the impact of the inclusion of H-bonding functional groups on the physico-chemical properties of UV-cured polyacrylic coatings. (See Table 1.)

Several studies probing the impact of network molecular structure on the diffusion of low molecular weight species have been reported. Macroscopic drug release studies are often used to infer network

diffusion properties [12–14], however, the connection to molecular scale phenomena is difficult. Fluorescence correlation spectroscopy (FCS) was used by Zustiak et al. to probe molecular diffusion in crosslinked PEG-based networks [15], and by Payet et al. for diffusion of dextran in chitosan networks [16]. Some FCS studies [15,17] suggest that the presence of hydrogen-bonding affects solute self-diffusion within the network. Unfortunately, FCS requires solute concentrations far lower than in real CDDSs [18]. In previous work [19] we described the impact of acrylate network crosslink density on molecular diffusivity. Using nuclear magnetic resonance (NMR) spectral analysis, relaxometry and diffusometry, the network was shown to slow molecular diffusion due to an 'absorption-desorption' equilibrium which persists even when the calculated network mesh size is significantly larger than the hydrodynamic size of the solute. On the other hand Siepmann et al. proposed mathematical models describing mass transport inside diffusion-ordered CDDSs with different geometric shapes [20], however these models are not applicable to the complicated topologies and morphologies of UV-cured acrylate networks. Hence, a systematic experimental study into the impact of tailoring chemical structure on the molecular diffusion and network properties of UV-cured polyacrylate hydrogels at applications-relevant solute concentrations would be of great importance for designing next-generation functional coatings.

In this study three polyacrylate-based networks containing polyethylene glycol-700-diacrylate (PEGDA-700) and three different monoacrylate *co*-monomers of different hydrogen bonding capability were synthesized by UV-initiated polymerization (see Table 1) allowing the effective H-bond capability of the networks to be tailored. After confirming high double bond conversion in all cases by FTIR and ^{13}C NMR, variable temperature ^{1}H NMR experiments were used to demonstrate the presence of H-bonding. DSC thermoporometry, Double Quantum (DQ) NMR and NMR relaxometry were applied to assess the impact of the different monomers, with differing H-bonding capability, on effective network mesh size and chain mobility. The drug-like entity Eosin Y and H_2O were then used to probe the diffusion properties of the networks by PFG-NMR. Eosin Y was selected as it is a well-understood substance used widely in biological study [21]. It has molecular structure containing a conjugated part and H-bonding groups that are similar to many drug molecules, in addition it is less toxic and its ^{1}H NMR is quite simple reducing spectral overlapping. $LiClO_4$ was added to the networks, as an H-bonding disruptor, to differentiate direct (solute-network) H-bonding effects on diffusivity from those arising from the host matrix. The microscopic self-diffusivities of Eosin Y and H_2O molecules, and the macroscopic membrane mass diffusivities of Eosin Y are discussed in relation to network chain mobility and effective network mesh size. Finally, a 'modified diffusion model' identifying the effective mesh is proposed to explain the diffusion of solutes within the networks containing H-bonding groups.

2. Material and methods

2.1. Sample preparation

Polyethylene glycol-700-diacrylate (PEGDA-700), Hexyl acrylate (HA), 4-Hydroxybutyl acrylate (HBA), 2-[[(butylamino)carbonyl]oxy] ethyl acrylate (BAC), Photo-initiator: 2,2-Dimethoxy-2-phenylacetophenone (DMPA) was used for the syntheses of networks. Eosin Y disodium salt was used as the diffusion probe. All the chemicals were obtained from Sigma Aldrich, and used without any further purification.

Networks were prepared by UV-curing the mixtures described in Table 2. The photo initiator was 10–20 mg of 2,2-Dimethoxy-2-phenylacetophenone (DMPA). The formulation was poured into a petri dish, and then the petri dish was passed through the UV-rig (Heraeus Noblelight Fusion UV Inc.'s F300S model, with I300MB irradiator which has a lamp power of 300 w/in (120 w/cm), 1800 watts total) 30 times. Afterwards the cured film was inverted, and was then passed through the UV-rig a further 30 times. The rim of the resulting film was cut off, and the remaining part, with a thickness around 1 mm, was used for all the tests.

To ensure that the expected network structures were formed during curing, ^{13}C MAS NMR and IR analyses were undertaken for all the samples [22]. The molecular weight of the hydrolyzed acrylate backbone chains was determined by gel permeation chromatography (GPC) analysis. Solution state ^{1}H NMR analysis was also carried out on the $CDCl_3$ extracts of the same samples to evaluate the extractable fraction of the network. Details of the analyses and the spectra acquired are included in SI. The double bond conversions for all the samples were very high, although slightly lower for samples with H-bonding monomers. ^{13}C NMR spectra showed that no side reactions occurred during the curing process. The amount of extractable compounds from these networks was found to be negligible (see Fig. S2), and no change was observed in the GPC analyses of these hydrolyzed polyacrylic acid backbone (Table 2) demonstrating that the polyacrylic acid (PAA) backbone chains length is largely unaffected by the presence of H-bonding monomers in the copolymer side chain.

2.2. Equilibrium Water Content (EWC)

The equilibrium water content (EWC) at room temperature was determined gravimetrically using the following relation;

$$EWC = 100 * \frac{(W_{wet} - W_{dry})}{W_{wet}} \quad (1)$$

After equilibrating samples in water for 3 days, pieces were removed, lightly blotted to remove excess surface water and then weighed to determine W_{wet}. The dry mass, W_{dry}, was determined after drying samples under vacuum at 80 °C for 6 h (samples reached a constant mass by this time). Measurements for each sample were performed in at least duplicate and the calculated EWC varied by less than 1%.

2.3. NMR analysis

For NMR analysis of loaded gels, the polymers were fully swollen in D_2O solutions of Eosin Y at 1 mg/mL, or in D_2O solutions of Eosin Y at 1 mg/ml and $LiClO_4$ at 2 mg/mL, as appropriate.

Solid-state magic angle spinning (MAS) ^{1}H NMR and ^{13}C NMR spectra on unloaded dried hydrogels were recorded on a Bruker Avance III 600 MHz spectrometer equipped with a Standard-Bore MAS probe. 4 mm MAS rotor (80 μL) was used with a spinning rate of 12 kHz. All the dry samples were measured by both single pulse excitation (SPE) and cross-polarization (CP) pulse sequences. The 90° pulse length was calibrated to be 2 μs. The spectra were recorded with two different cross-polarization times (τ_{cp}) of 0.5 ms and 10 ms, in order to distinguish between the rigid and soft parts of the material.

All the swollen networks loaded with Eosin Y were analyzed by high resolution (HR) MAS ^{1}H NMR. Typical concentrations for these chemicals are 1 mg/mL Eosin Y and 2 mg/mL $LiClO_4$. The experiments were performed using a HRMAS probe with 4 mm CRAMPS MAS rotor (12 μL) spinning at 6 kHz. Single pulse excitation (SPE) was used in this study with a calibrated 90° pulse length of 8.5 μs.

The longitudinal (T_1) and transverse (T_2) ^{1}H magnetization relaxation times of both unloaded and loaded swollen hydrogels were measured on Bruker Minispec MQ20 spectrometer operating at ^{1}H frequency of 20 MHz. A standard inversion recovery pulse sequence was used to determine T_1 relaxation. The T_2 relaxation decay was measured with the Hahn-echo (HE) pulse sequence, 90_x^{o}—τ_{HE}—180_y^{o}—τ_{HE}—(acquisition), where $\tau_{HE} \geq 35$ μs, as well as by single pulse excitation (SPE) which records the rapidly decaying T_2 relaxation component. In the HE experiment, an echo signal is formed after the second pulse in the HE with a maximum at time $t = 2\tau_{HE}$ after

Table 2
Sample formulation and characterization of unloaded-networks by FTIR, gel permeation chromatography, NMR relaxometry, DQ NMR and mechanical analyses.

Sample Label	Monomer Type	PEGDA:MA (molar ratio)	Conversion[i] (%)	EWC[ii] (wt%)	PAA[iii]			NMR relaxometry		DQ NMR
					M_n (kDa)	PDI	n(PAA)	$T_{2,\ short}^{sw}$ (μs)	M_{c+p} (g/mol)	D_{avg} (kHz)
PEG-HA	HA	1:1	92 ± 5	25.8	9.7	2.6	135	176	195	1.70
PEG-HBA	HBA	1:1	91 ± 5	31.1	9.9	2.1	139	165	182	1.82
PEG-BAC	BAC	1:1	90 ± 5	29.9	10.2	2.7	142	168	186	1.77

(i) Determined by FTIR. (ii) EWC: equilibrium water content. (iii) Determined by chromatography; M_n, number average molecular weight; PD, polydispersity; n (PAA), degree of polymerization (calculated from chromatography). $T_{2,\ short}^{sw}$, T_2 relaxation of fast decay component for swollen samples at 20 °C, the standard deviation is around 10%; M_{c+p}, mean molar mass between crosslinks and chain entanglements; D_{avg}, average residual dipolar coupling constant, the standard deviation is around 10%. GPC experimental details are provided in SI.

the first 90° pulse. By varying τ_{HE} the amplitude of the transverse magnetization, $A(t)$, was measured as a function of time, as detailed in our previous study [23].

The ^{1}H double-quantum (DQ) NMR experiments on unloaded dry networks were carried out on a Varian NMR Spectrometer 850 operating at a ^{1}H Larmor frequency of 849.71 MHz equipped with a 1.6 mm triple resonance probe. The MAS frequency was set to 40 kHz and the sample temperature to 50 °C. The 90° pulse length was calibrated to 2 μs. The data for all network samples was acquired using a recently published improved version of the Back-to-Back (BaBa) sequence [24], BaBa-xy16, for broadband homonuclear DQ recoupling [25]. Experiment details can be found in our previous publication [23]. Furthermore, all the varied temperature experiments were also carried out on this spectrometer. After being calibrated by ethylene glycol, these VT measurements were performed after equilibrating the sample at targeted temperature for 5 mins.

The PFG ^{1}H NMR measurements on Eosin Y loaded hydrogels were performed on Bruker AVANCE III HD 500 MHz Wide-Bore spectrometer (11.7 T wide bore super-conducting, ultra-shielded magnet). The spectrometer was equipped with a Diff50 diffusion probe, capable of reaching a maximum gradient strength of 30 T/m at 60 A. The self-diffusion coefficients were measured by implementing either a stimulated echo sequence, or a spin echo sequence in the case of samples with faster T_2 relaxation. All pulse sequences used sine shape gradient pulses with variable amplitudes. The signal attenuation can be described as;

$$\ln \frac{S}{S_0} = -\gamma g^2 \delta^2 \left(\Delta - \frac{\delta}{3}\right) D \tag{2}$$

Where S is the echo signal amplitude, S_0 is the signal amplitude at gradient strength $g = 0$, δ is the effective gradient pulse duration, Δ is the diffusion time, γ is the gyromagnetic ratio, and D is the diffusion coefficient. The experiments were performed at 37 °C. Diffusion experiments used different diffusion times (20, 40 or 100 ms) to demonstrate the absence of convection. The gradient was ramped in a linear fashion from 2 to 98% of full the gradient strength 30 G/cm/A. Two sine shaped gradient pulses of 1.1 ms duration was used for both coding and decoding. Typical acquisition parameters were as follows; 32 k acquisition points; 2.0 s recycle delay, 1 ms gradient pulse length (δ); 20 ms diffusion time (Δ); 0.2 ms gradient stabilization time; 10 kHz spectral width.

As noted above the PFG analysis was performed at EWC in D_2O. Water diffusion was assessed by monitoring the residual signal, *i.e.* primarily HOD. We will refer to this as the water response, and label the corresponding diffusion coefficients, D_{H_2O}. Under the conditions used, this resonance can be considered as arising from two components; a free state (4.6 ppm) and a "bound" state (4.9 ppm), the analysis was done by integrating the whole area under these two peaks. As discussed below, slow and fast diffusing components were then apparent. Note that due to the interaction between Eosin Y and the corresponding network, several additional peaks originated from the interaction between the solute molecules and polymer network appeared in the NMR spectrum (Fig. S13), as noted in our previous study [19].

All the varied temperature experiments were calibrated by ethylene glycol and performed after equilibrating the sample at targeted temperature for 5 mins.

2.4. Thermoporometry Analyses by Differential Scanning Calorimetry (DSC)

A representative fraction of the water swollen material (5–8 mg) was cut and placed into a hermetic DSC pan. DSC measurements were carried on a Q100 DSC apparatus from TA Instruments. DSC scans were recorded in heating mode with nitrogen as the purge gas. The pristine sample was cooled to below the melting point of ice and kept at the starting temperature (−40 °C) for 5 min before beginning the heating ramp of 0.5 °C/min to 10 °C, the samples were then kept at 10 °C isothermally for 10 min, and then slowly cooled down to −40 °C (0.5 °C/min). Because of the very broad distribution of ice crystallite's melting point as well as the water crystallization peak in the gel network, the starting temperature for date acquisition was chosen to be −40 °C, and the final temperature was 10 °C. The relevant methodology and the procedure to extract average pore (mesh) size are given in reference [26].

2.5. Permeation study of Eosin Y

A Side-By-Side diffusion cell (Crown Glass Company, Inc., Somerville, NJ) was used to analyze the diffusivity of Eosin Y across the films of cured acrylates networks using the time lag equations described by Crank [27]. The stirring rates of the stir-bars in both receptor and donor of the diffusion cell are 600 rpm. These films were equilibrated in de-ionised (DI) water before the experiments at room temperature overnight, and then placed between the halves of the permeation cell with an exposed area of 0.64 cm^2. The reason for equilibrating the film in DI water at room temperature is to record the permeation curve more accurately from the time point 0, as well as to reduce the deviation in fitting the permeation curve introduced by the inhomogeneous swelling of the network. Firstly, 3 mL of the DI water was added into the receptor cell, afterwards 3 mL of saturated Eosin Y disodium salt DI water solution containing excessive solid Eosin Y disodium salt was placed into the donor cell, and this was noted as zero time. The concentration of Eosin Y in the receptor cell's DI water solution was sampled every 30 mins and measured at Eosin Y's absorption band around 535 nm with a UV spectrometer. The thickness of the film was measured with a micrometer after equilibration in distilled water. In some experiments, an additional 2 mg/mL $LiClO_4$ DI water solution was added into both donor and receptor cells.

From these side-by-side diffusion cell experiments permeability coefficients were calculated from the data obtained using the following equation: [28,29].

$$\ln\left(1 - \frac{2C_t}{C_o}\right) = -\frac{2A}{V} Pt \tag{3}$$

Where C_t is the solute concentration in the receptor cell at time t; C_o

is the initial solute concentration of the donor cell; V is volume of each half-cell; A is the effective area of permeation; and P is the membrane permeability coefficient. To determine the permeability coefficient, P, a plot of $-(Vl/2A) \cdot \ln [1 - 2(C_t/C_0)]$ *versus* time, t, was constructed. The linear portion yields a slope of the permeability coefficient, P in m/s. Furthermore, the diffusion coefficient D_m, can also be calculated by:

$$D_m = \frac{Pl}{K_d} \quad (4)$$

Where l is the swollen membrane thickness, and K_d is the partition coefficient which is a ratio of solute concentration in the membrane to the solute concentration in the solution at the equilibrium.

3. Results

Three hydrogel samples were prepared, according to the procedure described above, the formulation details are provided in Table 2. These unloaded hydrogels were fully physically characterized prior to assessing the effect of the monomer type on the interactions with Eosin Y. The percentage of the HA, BAC, HBA monomer which are chemically crosslinked in the networks can be calculated by measuring the weight loss of the samples after repetitive swelling-deswelling of the cured gel samples. It was found that this value is less than 3% after 10 swelling-deswelling cycles (5 repetitions). On the other hand, if these free monomers are permanently physically entrapped in the networks, these fragments would be present as part of the slow relaxation component in the low field T_2 measurements, as shown in Fig. 3 and Fig. S7, the long tail part is less than 5%. Hence, we consider these networks used in this study were well-cured with negligible defects.

3.1. Hydrogen bonding in unloaded hydrogels

The presence of hydrogen bonding can be assessed by variable temperature ^{1}H NMR spectroscopy [30,31]. In Fig. 2 the changes in chemical shifts and spectral linewidths on varying the sample temperature are shown. For non-hydrogen bonding groups (*e.g.* the -CH_2- group in PEG) temperature had little effect on either the chemical shift or spectral linewidth. When hydrogen bonding groups are present, on increasing the temperature, the $\delta(^1H)$ for both –OH group in PEG-HBA and –NH group in PEG-BAC shifted to higher field, and the corresponding linewidths were consistently reduced. These changes can be explained as arising from the dynamics of H-bonding exchange [32]. Normally, such groups are in equilibrium between bonding and non-bonding states; at room temperature this exchange is usually relatively fast on the NMR time scale, therefore an averaged $\delta(^1H)$ for the two states is observed along with an increased linewidth. On increasing the temperature the bound state population decreases and the exchange rate increases resulting in a decrease in chemical shift and linewidth. These changes are consistent with previous studies in which bonds formed from –OH groups are found to be stronger than those from –NH groups [33], and similar conclusions can also be drawn from FTIR analyses of the N—H and O—H stretching modes, for details see Fig. S7. It is difficult to draw quantitative conclusions from these observations. However, for PEG-HBA the observed larger linewidth changes suggest greater H-bonding strength than in the case of PEG-BAC.

3.2. Network polymer chain dynamics in unloaded hydrogels

The introduction of hydrogen bonding into the polymer can induce structural or topological changes to the network [34–36]. As the networks studied here are formed from monomers with different H-bonding capability it is necessary to evaluate the extent of such changes and their influences in dynamics, prior to studying the effect of H-bonding on solute diffusion. However, DMA analysis demonstrates similar thermal response with expected higher T_g and lower storage modulus (E') in rubbery plateau for networks with H-bonding (see Fig. S6), note that the smaller E' for H-bond capable networks is due to a decrease in network density, as will be shown below. We have used ^{1}H NMR as it is a sensitive probe of the polymer network dynamics.

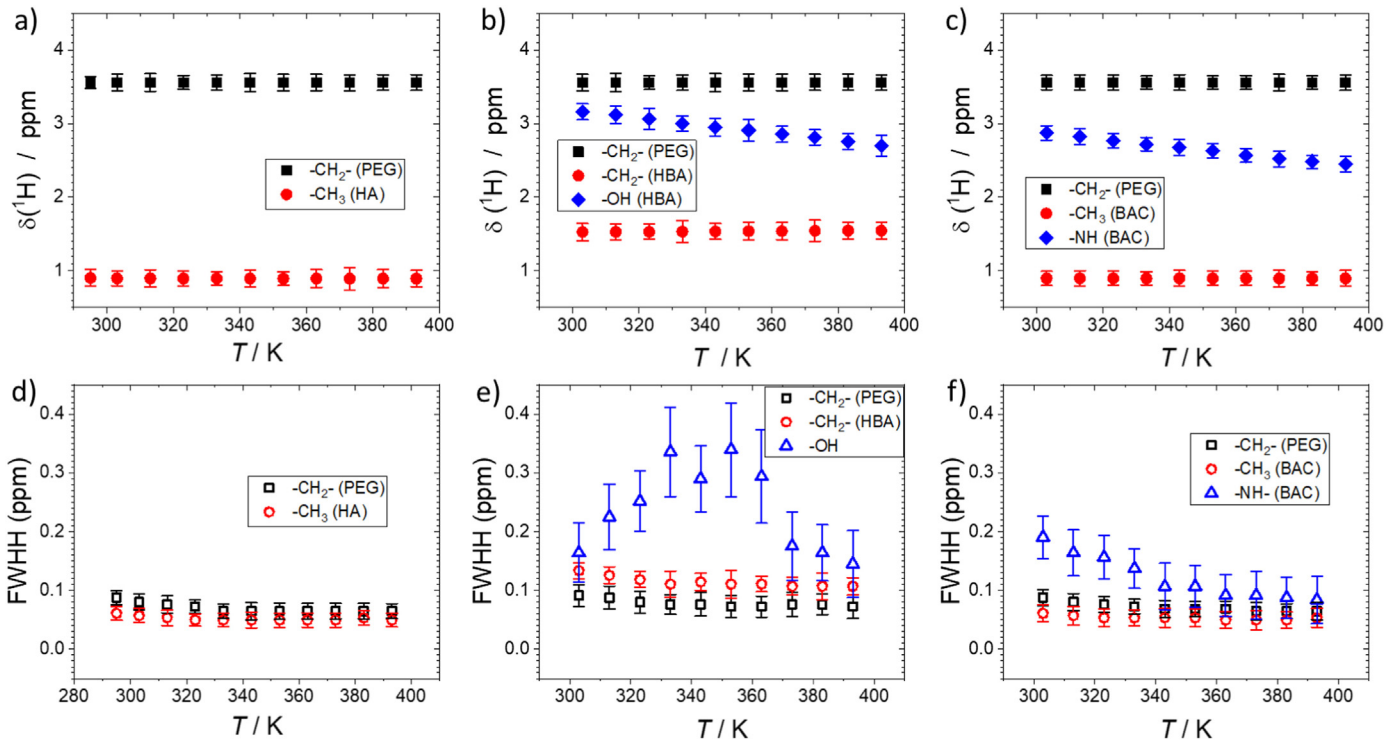

Fig. 2. Temperature dependence of the ^{1}H NMR chemical shifts (a, b, c) and the linewidths (e, f, g) for the unloaded polymer networks; (a, d) PEG-HA, (b, e) PEG-HBA, and (c, f) PEG-BAC. The response of the PEG unit, copolymer unit and -OH/-NH groups are included for comparison. FWHH is the full line width at half height. The error bars calculated from triplicate data sets.

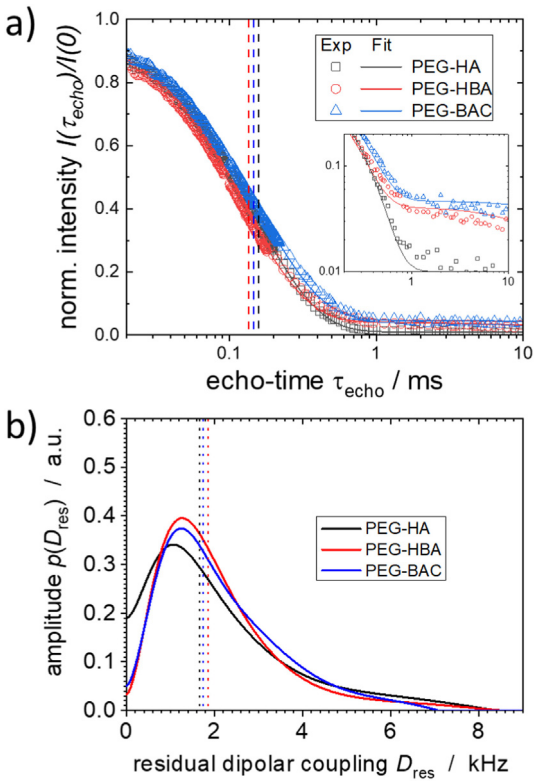

Fig. 3. ^{1}H NMR analysis of unloaded hydrogels: (a) ^{1}H NMR T_2 decay curves at 37 °C with the best-fit of the decay (solid lines) for PEG-HA (black), PEG-HBA (red), and PEG-BAC (blue). Vertical dash-lines indicate relaxation time $T_{2,\ short}^{sw}$. of the decays at the longer echo-time range are shown on the insert; (b) Distribution of residual dipolar coupling constant D_{res} for PEG-HA (black), PEG-HBA (red), and PEG-BAC (blue) at 37 °C. The dotted-lines indicate the average residual dipolar coupling constant, D_{avg}. (For interpretation of the references to colour in this figure legend, the reader is referred to the web version of this article.)

^{1}H NMR T_2 relaxation is very sensitive to polymer chain dynamics, hence even small differences in network structure and heterogeneity can often be identified from the relaxation response [23,37]. As shown in Fig. 3a, similar T_2 decays were observed for all three networks. For all samples after chloroform extraction, two components with distinguishable relaxation times can be identified in the analysis, as shown in Table 2 and Table S2 in SI, using the fitting procedure described previously [23,37–39]. PEG-HBA shows the smallest value for the fast-relaxing component ($T_{2,\ short}^{sw}$), which we tentatively assign to main network chain dynamics, indicative of slightly more restricted chain mobility compared to the other two networks. The presence of H-bonding groups was found to result in a slight increase in the fraction of the slowly relaxing component, which can be associated with the number of network defects and dangling chains. (Fig. 3a and Fig. S8). However, there is no evidence that H-bonding groups significantly alter network structure. Finally, T_2 measurements also demonstrate (Fig. S9) that the addition of Eosin Y (selected as it has functional groups that can take part in H-bonding) at *ca.* 1 mg/mL does not significantly change the chain dynamics for all the networks studied.

Double quantum (DQ) NMR was also used to evaluate differences in chain dynamics in the samples [40]. In this experiment, by varying the duration of homonuclear dipolar recoupling pulse sequence, the evolution of double-quantum coherences (DQCs, states involving pairs of dipole-dipole coupled ^{1}H nuclei) can be recorded. DQC buildup curves are shown for the PEG unit in Fig. S10, from which residual dipolar coupling constant (D_{res}) distributions can be extracted, the results are shown in Fig. 3b. All three samples have very similar D_{res} distributions demonstrating the similarities of the network structure. PEG-HBA shows slightly larger average coupling constant, D_{avg}, indicating slightly more restrained PEG chain dynamics in this network consistent with the T_2 analysis. These results show a relatively weak effect of H-bonding monomer on network dynamics.

3.3. Effective network mesh size of unloaded hydrogels

The mesh sizes of the unloaded networks were evaluated by DSC thermoporometry to assess the effect of the change in formulation on the pore structure of the resulting networks [44,45]. Using this method the effective mesh radius, R_m, can be determined (see Fig. S11) from the exothermic melting peak of ice crystals within the mesh by [41]:

$$R_m = -\frac{64.67}{\Delta T} + 0.57 \tag{5}$$

where $\Delta T = T - T_0$ is the shift in the triple point, here we use the shifting of the melting temperature of ice crystals. The mesh size distribution curve can be determined from:

$$\frac{\Delta V}{\Delta R_m} = \frac{k}{64.67}\frac{\Delta T^2}{W_a}Y \tag{6}$$

where V is the volume of the hydrogel, k is a factor that depends on the rate of cooling and weight of the sample (here $k = 33.32$ K·nm), the apparent energy of solidification of water $W_a = -5.56 \times 10^{-2}\Delta T^2 - 7.43\Delta T - 332$, Y is the heat flow. The resulting effective mesh radius distribution curves are shown in Fig. 4a; it was found that the mesh size increased when comparing PEG-HA to PEG-BAC and was it larger again for PEG-HBA, with values of 11.2, 12.9 and 14.1 nm obtained, respectively. Increases in the average mesh size are often correlated with decreases in the network polymer chain mobility [42], and it known that the presence of H-bonding can reduce the chain mobility in polymer networks [43,44]. However, as shown by the NMR analyses, there is little difference in $T_{2,\ short}^{sw}$ or D_{res} for these samples. The implications are discussed below.

The effective average mesh size (ξ_{avg}), can also be determined from the swelling degree using the Peppas approach [45]. Full details of the calculations are given in SI, and the values obtained are plotted, along with R_m, in Fig. 4b. The ξ_{avg}values obtained were typically only one third of those obtained from thermoporometry measurements. This is not surprising that the Peppas approach is only strictly applicable to homopolymers with Gaussian chain dynamics. It is interesting that the experimental trend in average mesh size is also reproduced by these calculations. Since H-bonding effects are not included in the swelling calculations, the observed consistency with thermoporometry suggests that values from the latter are only weakly influenced by contributions from H-bonding and that they are relevant to interpreting network responses measured at room temperature.

3.4. Diffusion of Eosin Y in hydrogels

PFG-NMR is an established method to measure effective solute self-diffusion in heterogeneous environments such as polyacrylate networks [19]. The Eosin Y and water self-diffusion coefficients within the swollen hydrogels (at equlibrium swelling state in H_2O) were measured at 298 K, with and without added H-bonding disruptor $LiClO_4$ [46,47] (at 2 mg/mL close to its solubility limit) to evaluate any effect of H-bonding on solute-polymer chain interactions. The PFG NMR diffusion measurement in this study are volume average measurements in the fast dynamic regime. According to classic theory of diffusion in porous materials, there are generally two (sometimes even three) diffusion components of small molecules in these systems, one representing the surface interaction between the pore and the diffusor, the other is the diffusion in the bulky reservoir area. The presence of loose structure (*e.g.* network defects, loops) would reduce the surface area to volume ratio. However, since the percentage of any loose parts in the network is

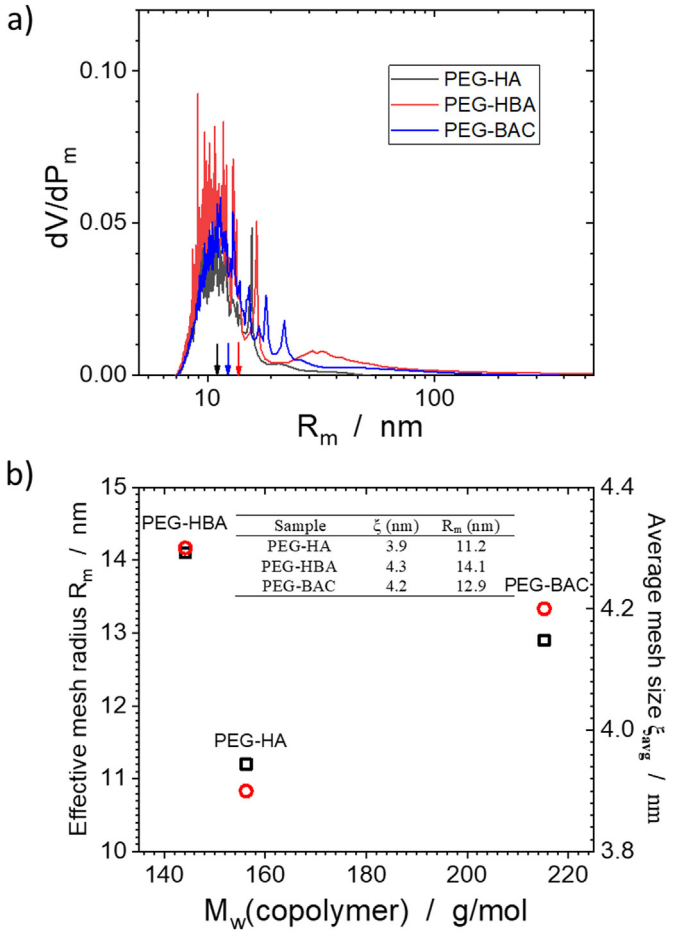

Fig. 4. Pore size analysis of unloaded hydrogels shown here (to distinguish between the samples) as a function of copolymer M_w. (a) Mesh volume distribution dV/dR_m ($cm^3/g{\cdot}nm$) *versus* effective mesh radius, R_m (nm), determined from DSC thermoporometry; (b) Comparison between the effective mesh radius, R_m, and the average mesh size ξ_{avg}.

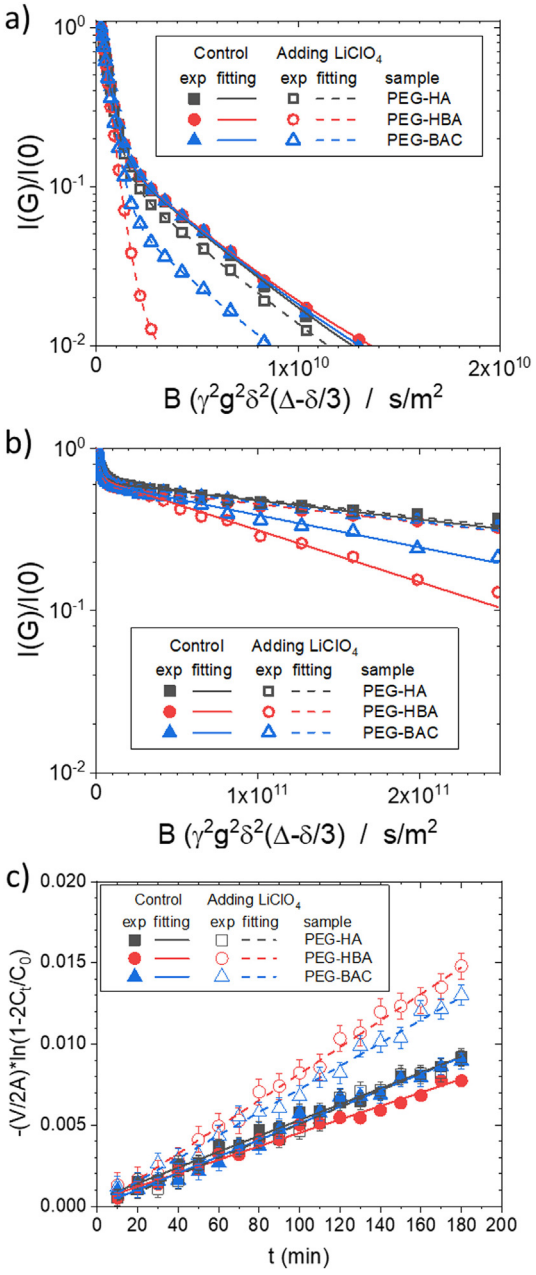

Fig. 5. (a-b) Stejslak-Tanner plots for Eosin Y loaded hydrogels. ^{1}H PFG responses is recorded at 298 K for (a) water and (b) Eosin Y (*ca.*1 mg/mL) self-diffusion in networks. (c) Permeation behavior of Eosin Y in the networks. PEG-HA (black), PEG-HBA (blue) and PEG-BAC (red) with (solid) or without (hollow) $LiClO_4$ (2 mg/mL).

relatively small (see Fig. 3), we consider its effect on the overall diffusion data to be negligible, and extract two components form the diffusion data.

Fig. 5a and b display the attenuation of the ^{1}H signal intensity during the PFG-SE experiments for water and Eosin Y in all the networks, respectively. H_2O was used to probe the diffusion properties alongside Eosin Y to evaluate the impact of the size of solute on H-bonding effects in these networks. Smaller molecules like H_2O should be less affected by the indirect H-bonding effect (H-bonding induced reduction in mesh size). Hence by evaluating the change in diffusion coefficient of Eosin Y and H_2O after introducing a chaotropic reagent, we can semi-quantitatively separate the direct from the indirect H-bonding effect. Two distinguishable translational diffusion components can be observed in every case indicating the presence of interactions between the networks and the diffusing species (water and Eosin Y). The slower diffusing component is assigned to restricted molecular diffusion inside the polymer network ($D_{X,\,b}$) in which the solute interacts with the network and therefore exhibits a reduced diffusion coefficient, while the faster one ($D_{X,\,f}$) is assigned to free diffusion of the solute in the pure solvent (water). As in the case of the chemical shifts, the diffusion of water and Eosin Y in the hydrogels can be described as an absorption-desorption equilibrium between the diffusor and the network [48]. The extracted diffusion coefficients are summarized in Table 3. Both solutes show reduced translational self-diffusion coefficients in comparison to their free diffusing counterparts. $D_{H2O,\,b}$ is found to be lower than $D_{H2O,\,f}$ by almost an order of magnitude, while $D_{EY,\,b}$ decreases by more than two orders of magnitude compared to its free counterpart, $D_{EY,\,f}$. This difference can be attributed primarily to the greater size of Eosin Y ($r = 0.7\ nm$) compared to water ($r = 0.2\ nm$), which in turn reduces its mobility, particularly given the relatively small mesh sizes in these networks, see Fig. 4. As noted above, low field relaxometry shows no significant effect of Eosin Y on the network dynamics (Fig. S9), so only effects of H-bonding and mesh size need be considered. In this case, a stronger H-bonding effect is suggested for both PEG-HBA and PEG-BAC networks as lower $D_{EY,\,b}$ values were measured for themcompared to PEG-HA.

Upon adding $LiClO_4$, the $D_{H2O,\,f}$ values were unchanged, as expected, but $D_{EY,\,f}$ increased. This increase for free Eosin Y can be interpreted as arising from disruption of Eosin Y aggregates by $LiClO_4$. Aggregation of Eosin Y arises from hydrophobic interactions between

Table 3
Self-diffusion coefficients at 298 K of Eosin Y and water for Eosin Y loaded hydrogels with or without $LiClO_4$, measured using ^1H PFG NMR diffusometry, as well as $D_{M,\ EY}$ measured by a conventional permeation study. The uncertainties are estimated from triplicate measurements to be *ca.*10% in all cases.

Network	*Free*		*Bound*		$D_{M,\ EY}$ (m^2/s)
	$D_{EY,\ f}$ (m^2/s)	$D_{H_2O,\ f}$ (m^2/s)	$D_{EY,\ b}$ (m^2/s)	$D_{H_2O,\ b}$ (m^2/s)	
PEG-HA	3.8×10^{-10}	2.5×10^{-9}	6.1×10^{-12}	3.2×10^{-10}	2.6×10^{-11}
PEG-HA (+ $LiClO_4$)	6.1×10^{-10}	2.4×10^{-9}	6.1×10^{-12}	3.2×10^{-10}	2.8×10^{-11}
PEG-HBA	3.6×10^{-10}	2.4×10^{-9}	3.6×10^{-12}	3.2×10^{-10}	2.5×10^{-11}
PEG-HBA (+ $LiClO_4$)	6.1×10^{-10}	2.4×10^{-9}	13.0×10^{-12}	4.5×10^{-10}	5.1×10^{-11}
PEG-BAC	3.6×10^{-10}	2.4×10^{-9}	4.2×10^{-12}	3.2×10^{-10}	2.5×10^{-11}
PEG-BAC (+ $LiClO_4$)	6.1×10^{-10}	2.4×10^{-9}	7.8×10^{-12}	3.8×10^{-10}	4.4×10^{-11}

individual Eosin Y molecules, the chaotropic agent, $LiClO_4$ is known to disrupt this type of aggregation [49]. Diffusion measurements on pure Eosin Y solutions (see Fig. S12) confirmed Eosin Y aggregation.

The dependence of $D_{EY,\ b}$ on $LiClO_4$ is particularly interesting. No change in this value was measured for PEG-HA demonstrating that this Eosin Y fraction exists predominantly in monomer form in the networks, probably due to disruption of any Eosin Y assemblies by the polymer chains, and that there is no strong H-bond interaction between Eosin Y and the PEG-HA network. On the other hand, increases in $D_{EY,\ b}$ were observed on adding $LiClO_4$ for PEG-HBA and PEG-BAC, of close to 4- and 2-fold, respectively, demonstrating the presence of H-bonding interactions between Eosin Y and the polymer chains restricting solute diffusion, and this change is greater in the former as its H-bonding strength is greater. The effect of $LiClO_4$ on $D_{H2O,\ b}$ was weak in all cases. Apparently the average mesh sizes of these networks are too large, given that water is a considerably smaller molecule than Eosin Y, for local interactions to alter water diffusivity significantly. Although it should be noted that it is anticipated that direct H-bonding interactions between H_2O and networks would also be weaker. PEG-HBA was an exception with a ~ 30% $LiClO_4$-induced increase, interestingly this network is also found to have the biggest $LiClO_4$ induced increase in $D_{EY,\ b}$ as well as the biggest average mesh size R_m. This relationship will be discussed later in detail.

A traditional permeation study was also performed on membranes formed from these materials as the permeability can be closely related to the diffusive properties of the membrane [50]. As shown in Fig. 5c and Table 3, the overall Eosin Y mass diffusivity, $D_{M,\ EY}$, values were similar, *c.*$2\sim3 \times 10^{-11}$ m^2/s for the three samples, which is in the range typically for the conditions studied [51], and is consistent with the films being homogeneously cured. An increase in $D_{M,\ EY}$ was observed for all the networks on adding $LiClO_4$, this was particularly strong for the H-bond containing systems, demonstrating that H-bonding disruption at a microscopic level also affects the bulk sample response. Furthermore, as was the case for Eosin Y diffusivity, the elimination of H-bonding effects resulted in a positive correlation between the $D_{M,\ EY}$ and average network mesh size R_m. Similar correlations have been described previously for PEG networks [29].

In summary, it was found that the water diffusivity within the networks was reduced by an order of magnitude as compared to the 'free' water, while the diffusivity of Eosin Y decreased by about two orders of magnitude, due to network mesh size restrictions. For networks with H-bonding containing monomers, NMR diffusometry showed that; (i) direct H-bonding interactions between solute and network are significant and can moderate solute diffusion; (ii) this effect is monomer dependent, therefore it is possible to tailor it; (iii) the effect can be attenuated by the addition of a chaotropic reagent; (iv) the microscopic diffusivity is correlated with the membrane macroscopic mass diffusivity.

4. Discussion

4.1. Influence of hydrogen bonding on hydrogel polymer dynamics

The striking differences in diffusivity (with and without disruptor) apart the physical properties of the networks are apparently quite similar; however this aspect is worth some further consideration. Additional information about the network structure can be obtained by analyzing the mean molar mass between crosslinks, chain entanglements and physical junctions, M_{c+p}. Assuming Gaussian chain statistics and the Affine Model (in which the deformation of each polymer chain in the network is the same as the macroscopic deformation) are applicable, as was shown to be reasonable for UV-cured polyacrylate networks in our previous study [40], M_{c+p} can be calculated from the $T_{2,\ short}{}^{sw}$ values recorded in the swollen state [23]. M_{c+p} can also be approximated to be inversely proportional to the average residual dipolar coupling constant, D_{avg}. As shown in Fig. 6a, the M_{c+p} and $1/D_{avg}$ values obtained from these two approaches are strongly correlated, suggesting the two properties, measured by different techniques, are sensitive to the same dynamics. It is also found that the M_{c+p} (and hence $1/D_{avg}$) values are weakly inversely correlated with the average mesh size R_m. This is interesting as Flory Theory suggests that the mean molar mass between crosslinks should systematically increase with R_m [45,52]. As suggested by a previous study [36], this phenomenon can be explained by a possible pre-organization of H-bonding containing monoacrylates during UV curing, which in turn accelerates the curing reaction rate while also promoting formation of H-bonded physical junctions. Hence, we suggest that in this case H-bonding reduces chain mobility by increasing the number of physical junctions which reduces M_{c+p}. Similar effects have been reported previously for thermoplastic elastomers [53] and as well as for polymer-silica nanocomposites [54].

4.2. Influence of hydrogen bonding on solute diffusion

Conventionally free volume and average mesh size effects are considered to be critical in crosslinked hydrogels with microscopic mesh sizes (2–50 nm) when the diffusing solute is of considerably smaller size [55]. By plotting self-diffusion coefficients for both Eosin Y and H_2O as a function of the effective mesh radius (Fig. 6b), it is clear that the diffusivity of these solutes does not increase with R_m in the absence of the chaotropic reagent. However, a positive correlation is established on adding $LiClO_4$. This correlation is more prominent for larger solute molecule due to stronger mesh size induced restrictions [55]. As a chaotropic reagent, lithium perchlorate can disrupt the formation of non-covalent bonds. In this case it acts as a H-bond acceptor and has stronger donor-acceptor interactions with the network –OH/-NH-groups [56], disrupting H-bonding between polymer chains and Eosin Y but also between polymer chains. Hence we suggest that the chaotropic agent disrupts direct H-bonding interactions, transforming the solutes' diffusion within the networks into a normal mesh-size dependent process, in which diffusivity increases with increasing mesh size, as is observed for non-hydrogen bonding networks [57,58]. Given the strong

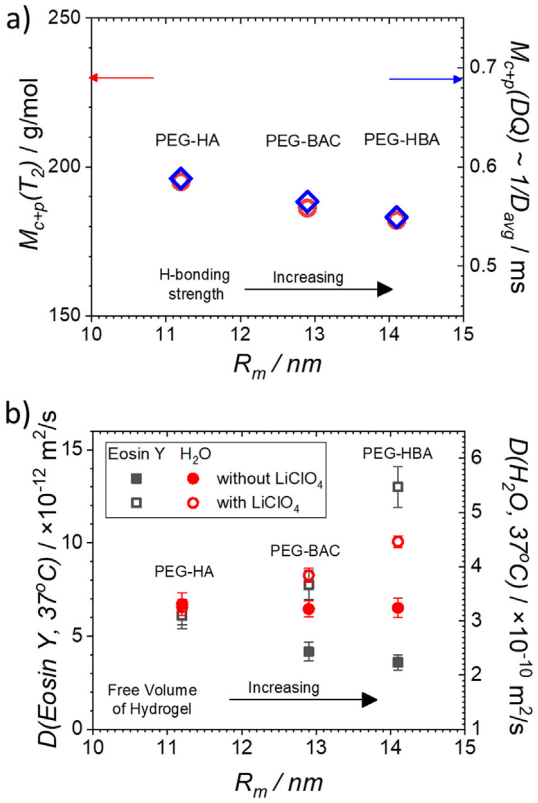

Fig. 6. (a) Mean molar mass between crosslinks, chain entanglements and physical junctions, M_{c+p}, for the unloaded networks from NMR relaxometry (red) and DQ NMR (blue) as a function of R_m, which is determined by DSC thermoporometry. (b) Diffusion coefficients (at 310 K) of Eosin Y (black) and H_2O (red) in the networks, as a function of effective mesh radius, R_m. (For interpretation of the references to colour in this figure legend, the reader is referred to the web version of this article.)

evidence for H-bonding provided by the ^{1}H spectra (Fig. S13) we conclude that direct (solute-network) hydrogen bonding is a key factor.

4.3. Solute diffusion model for hydrogen bond containing networks

Due to the complicated nature of solute diffusion processes inside hydrogel networks, many models have been proposed [55,59]. As discussed by Amsden [59], among all the models developed for mesoscopically homogenous gels, Cukier's Model, is one of the most reliable. This is a hydrodynamic approach to quantitatively estimating the hydrodynamic interaction between the solute and network [59,60] which relates the relative diffusivity in the gel to the extent and spatial range of the hydrodynamic interactions. Since all the networks in current study are mesoscopically homogenous, as shown by (DQ) NMR, we will adopt Cukier' Model, which describes:

$$\frac{D_g}{D_0} = exp(-k_c r_s \varphi^{0.75}) \tag{7}$$

where D_g is the solute diffusivity in the gel, D_0 is the solute diffusivity in the liquid at infinite dilution, r_s is the hydrodynamic size of the solute (2.75 Å for water, 7.1 Å for Eosin Y) [61], φ is the polymer volume fraction in hydrogel (determined here from the EWC), and k_c is a constant for a given polymer-solvent system, which represents the screening hydrodynamic interaction between the solute and the polymer network [55].

The calculated values of k_c for all the samples are listed in Table 4, the values are in a similar range to those previously reported for other acrylate networks [59,62]. Increasing H-bonding strength in the network can be seen to be associated with an increase in k_c, indicating an increased affinity between the network and solute. Moreover, the decrease in k_c value for H-bond containing networks after the addition of $LiClO_4$ suggests that the chaotrope significantly affects the hydrodynamic interaction between the hydrogel and solute. Based on the above discussion, here we introduce a new term, ϵ, into the classical Cukier's Model, which is proportional to the strength of the hydrodynamic interaction in the corresponding network, hence the equation can be written as:

$$\frac{D_g}{D_0} = exp(-k'_c r_s \varphi^{0.75}\epsilon) \tag{8}$$

where $k'_c = k_c/\epsilon$, which can be considered as the normal hydrodynamic interaction between solute and network without the direct influence of H-bonding. Assuming the inclusion of chaotropic reagents into the system completely disturbs the hydrogen bonding based interaction, the value of ϵ can be directly calculated using the two k_c value obtained with and without $LiClO_4$, and k'_c can then also be extracted. As expected, ϵ is found to increase with increasing H-bonding strength, since stronger H-bonding increase the hydrodynamic interaction, as suggested by previous studies [63]. On the other hand, k'_c represents the hydrodynamic interaction between the network and solute excluding direct H-bonding interactions. As shown in Table 4, k'_c is found to be positively correlated with R_m, the average mesh size of the network. Hence we suggest that the parameters k'_c and ϵ may indicate the two aspects of the total effective interaction for Eosin Y. By carefully analyzing the diffusometry with a suitable hydrodynamic theory based diffusion model, we suggest that it is possible to separate the solute-hydrogel interaction (*direct H-bonding effect*) from H-bonding induced reduction in the average network mesh size (*indirect H-bonding effect*).

5. Conclusions

In this study, the self-diffusion coefficients of Eosin Y and water inside a series of modified polyacrylate networks were measured by NMR diffusometry. Eosin Y was selected as it is a well-understood low molecular weight H-bond capable drug-like substance commonly applied in biology. It was found that solute (Eosin Y and water) diffusivity was affected by the presence of monomers with H-bonding capability. In addition to direct molecular H-bonding interactions between the solute and the network chains, the mesh size of the networks was also altered indirectly by the presence of hydrogen bonding due to preorganization effects, which themselves contribute to solute diffusivity. The introduction of a chaotropic agent resulted in the anticipated positive correlation between solute self-diffusivity and average mesh size for H-bond capable networks, conforming with the predictions of conventional hydrodynamic theory for diffusion, and arising due to suppression of the direct H-bond interaction. Hence we propose a modified diffusion model based on hydrodynamic theory, in which one can separately analyze these two contributions. Since Cukier's model is valid in physiological conditions [64,65] the modified Cukier model shown here should also be applicable to more complex environments though the ϵ value may change due to differences in pH.

This work provides physical insights into diffusivity of low molecular weight species in networks and demonstrates how molecular diffusion and release processes in CDDSs can be tailored through selection of monomers and active disruption of H-bonding. Critically, it also demonstrates that the effects which modulate microscopic diffusion also determine the bulk permeability of membranes cast from the same formulations. Finally it identifies the likely effects of environmental chaotropes on the release profiles of H-bond capable CDDSs when placed in biological environments.

Studies using physiological environments and different drug molecules will be needed to develop predictive model for CDDSs. Experiments using different physiological environments and real drugs carrying fluorine tags (^{19}F NMR diffusometry) in which these issues will be addressed are ongoing. The current work clarifies key aspects of

Table 4
k_c and ϵ values, determined using Cukier's Model, for Eosin Y and water diffusivity in hydrogels with and without the addition of $LiClO_4$ (*ca.*2 mg/mL).

Sample	Eosin Y			Water		
	Without $LiClO_4$	With $LiClO_4$	ϵ	Without $LiClO_4$	With $LiClO_4$	ϵ
	k_c	k'_c		k_c	k'_c	
PEGDA-HA	0.87 ± 0.03	0.87 ± 0.03	1.00	0.81 ± 0.05	0.81 ± 0.05	1.00
PEGDA-HBA	0.95 ± 0.02	0.69 ± 0.07	1.38	0.95 ± 0.05	0.78 ± 0.03	1.22
PEGDA-BAC	0.89 ± 0.03	0.79 ± 0.05	1.13	0.94 ± 0.05	0.80 ± 0.03	1.18

molecular interactions that determine local diffusivity and bulk permeability providing both the fundamental understanding and experimental framework necessary for developing H-bond modulate-able CDDSs.

Acknowledgements

The research received financial support from EU FP7 Marie Curie Actions under the NEOGEL project (Grant No. 316973), the EU Horizon2020 Marie Curie Cofund project (Grant No. 713279), and Science Foundation Ireland (Grant Agreement No. 16/IA/4584).

Appendix A. Supplementary data

Supplementary data to this article can be found online at https://doi.org/10.1016/j.jconrel.2020.07.039.

References

[1] R. Langer, New methods of drug delivery, Science 249 (1990) 1527–1533.
[2] R. Langer, Drug delivery and targeting, Nature 392 (1998) 5–10.
[3] S.V. Sastry, J.R. Nyshadham, J.A. Fix, Recent technological advances in oral drug delivery - a review, Pharm Sci Technolo Today 3 (2000) 138–145.
[4] K.S. Soppimath, T.M. Aminabhavi, A.R. Kulkarni, W.E. Rudzinski, Biodegradable polymeric nanoparticles as drug delivery devices, J. Control. Release 70 (2001) 1–20.
[5] J. Jagur-Grodzinski, Polymers for tissue engineering, medical devices, and regenerative medicine. Concise general review of recent studies, Polym Advan Technol 17 (2006) 395–418.
[6] G. Acharya, K. Park, Mechanisms of controlled drug release from drug-eluting stents, Adv Drug Deliver Rev 58 (2006) 387–401.
[7] P. Colombo, R. Bettini, G. Massimo, P.L. Catellani, P. Santi, N.A. Peppas, Drug diffusion front movement is important in drug-release control from Swellable matrix tablets, J. Pharm. Sci. 84 (1995) 991–997.
[8] T.U. Okarter, K. Singla, The effects of plasticizers on the release of metoprolol tartrate from granules coated with a polymethacrylate film, Drug Dev. Ind. Pharm. 26 (2000) 323–329.
[9] Q.W. Yang, M.P. Flament, F. Siepmann, V. Busignies, B. Leclerc, C. Herry, P. Tchoreloff, J. Siepmann, Curing of aqueous polymeric film coatings: importance of the coating level and type of plasticizer, Eur. J. Pharm. Biopharm. 74 (2010) 362–370.
[10] Y. Yagci, S. Jockusch, N.J. Turro, Photoinitiated polymerization: advances, challenges, and opportunities, Macromolecules 43 (2010) 6245–6260.
[11] T.R. Hoare, D.S. Kohane, Hydrogels in drug delivery: Progress and challenges, Polymer 49 (2008) 1993–2007.
[12] L.C. Dong, A.S. Hoffman, A novel-approach for preparation of Ph-sensitive hydrogels for enteric drug delivery, J. Control. Release 15 (1991) 141–152.
[13] N.A. Peppas, S.L. Wright, Drug diffusion and binding in ionizable interpenetrating networks from poly(vinyl alcohol) and poly(acrylic acid), Eur. J. Pharm. Biopharm. 46 (1998) 15–29.
[14] N.A. Peppas, P. Colombo, Analysis of drug release behavior from swellable polymer carriers using the dimensionality index, J. Control. Release 45 (1997) 35–40.
[15] S.P. Zustiak, H. Boukari, J.B. Leach, Solute diffusion and interactions in cross-linked poly(ethylene glycol) hydrogels studied by fluorescence correlation spectroscopy, Soft Matter 6 (2010) 3609–3618.
[16] L. Payet, A. Ponton, L. Leger, H. Hervet, J.L. Grossiord, F. Agnely, Self-diffusion in chitosan networks: from a gel-gel method to fluorescence recovery after Photobleaching by fringe pattern, Macromolecules 41 (2008) 9376–9381.
[17] H.S. Park, J.M. Sung, T.H. Chang, Hydrogen bonding effect on probe diffusion in semidilute polymer solutions: polymer chain structure dependence, Macromolecules 29 (1996) 3216–3219.
[18] S.T. Hess, S.H. Huang, A.A. Heikal, W.W. Webb, Biological and chemical applications of fluorescence correlation spectroscopy: a review, Biochemistry-Us 41 (2002) 697–705.
[19] K. Tomic, W.S. Veeman, M. Boerakker, V.M. Litvinov, A.A. Dias, Lateral and rotational mobility of some drug molecules in a poly(ethylene glycol) diacrylate hydrogel and the effect of drug-cyclodextrin complexation, J. Pharm. Sci. 97 (2008) 3245–3256.
[20] J. Siepmann, F. Siepmann, Modeling of diffusion controlled drug delivery, J. Control. Release 161 (2012) 351–362.
[21] P. Kozlowski, S.D. Chang, E.C. Jones, K.W. Berean, H. Chen, S.L. Goldenberg, Combined diffusion-weighted and dynamic contrast-enhanced MRI for prostate cancer diagnosis - correlation with biopsy and histopathology, J. Magn. Reson. Imaging 24 (2006) 108–113.
[22] B. Wu, A. Sufi, R.G. Biswas, A. Hisatsune, V. Moxley-Paquette, P. Ning, R. Soong, A.P. Dicks, A.J. Simpson, Direct conversion of McDonald's waste cooking oil into a biodegradable high-resolution 3D-printing resin, ACS Sustain. Chem. Eng. 8 (2020) 1171–1177.
[23] B. Wu, W. Chasse, R. Peters, T. Brooijmans, A.A. Dias, A. Heise, C.J. Duxbury, A.P.M. Kentgens, D.F. Brougham, V.M. Litvinov, Network structure in acrylate systems: effect of junction topology on cross-link density and macroscopic gel properties, Macromolecules 49 (2016) 6531–6540.
[24] M. Feike, D.E. Demco, R. Graf, J. Gottwald, S. Hafner, H.W. Spiess, Broadband multiple-quantum NMR spectroscopy, J. Magn. Reson. Ser. A 122 (1996) 214–221.
[25] K. Saalwachter, F. Lange, K. Matyjaszewski, C.F. Huang, R. Graf, BaBa-xy16: robust and broadband homonuclear DQ recoupling for applications in rigid and soft solids up to the highest MAS frequencies, J. Magn. Reson. 212 (2011) 204–215.
[26] M.R. Landry, Thermoporometry by differential scanning calorimetry: experimental considerations and applications, Thermochim. Acta 433 (2005) 27–50.
[27] J. Crank, The Mathematics of Diffusion, 2d ed., Clarendon Press, Oxford, Eng, 1975.
[28] R.M. Ottenbrite, S.W. Kim, Polymeric drugs & drug delivery systems, Technomic Pub, Lancaster, Pa, 2001.
[29] J.L. Stringer, N.A. Peppas, Diffusion of small molecular weight drugs in radiation-crosslinked poly(ethylene oxide) hydrogels, J. Control. Release 42 (1996) 195–202.
[30] T.G. Pedersen, B.W. Sigurskjold, K.V. Andersen, M. Kjaer, F.M. Poulsen, C.M. Dobson, C. Redfield, A nuclear-magnetic-resonance study of the hydrogen-exchange behavior of lysozyme in crystals and solution, J. Mol. Biol. 218 (1991) 413–426.
[31] S.H. Gellman, G.P. Dado, G.B. Liang, B.R. Adams, Conformation-directing effects of a single intramolecular amide-amide hydrogen-bond - variable-temperature Nmr and Ir studies on a homologous Diamide series, J. Am. Chem. Soc. 113 (1991) 1164–1173.
[32] S. Scheiner, Hydrogen Bonding a Theoretical Perspective, Oxford University Press, New York etc, 1997.
[33] G.A. Jeffrey, An Introduction to Hydrogen Bonding, Oxford University Press, New York, 1997.
[34] X.D. Wang, X. Luo, A polymer network based on thermoplastic polyurethane and ethylene-propylene-diene elastomer via melt blending: morphology, mechanical properties, and rheology, Eur. Polym. J. 40 (2004) 2391–2399.
[35] X.Z. Yan, S.J. Li, J.B. Pollock, T.R. Cook, J.Z. Chen, Y.Y. Zhang, X.F. Ji, Y.H. Yu, F.H. Huang, P.J. Stang, Supramolecular polymers with tunable topologies via hierarchical coordination-driven self-assembly and hydrogen bonding interfaces, Proc. Natl. Acad. Sci. U. S. A. 110 (2013) 15585–15590.
[36] J.F.G.A. Jansen, A.A. Dias, M. Dorschu, B. Coussens, Fast monomers: factors affecting the inherent reactivity of acrylate monomers in photoinitiated acrylate polymerization, Macromolecules 36 (2003) 3861–3873.
[37] V.M. Litvinov, M. van Duin, Real-time H-1 NMR relaxation study of EPDM vulcanization, Kaut Gummi Kunstst 55 (2002) 460–463.
[38] M.G. Brereton, I.M. Ward, N. Boden, P. Wright, Nature of the proton Nmr transverse relaxation function of polyethylene melts.1. Monodispersed Polyethylenes, Macromolecules 24 (1991) 2068–2074.
[39] V.M. Litvinov, M.E. Ries, T.W. Baughman, A. Henke, P.P. Madoka, Chain entanglements in polyethylene melts. Why is it studied again? Macromolecules 46 (2013) 541–547.
[40] K. Saalwachter, Proton multiple-quantum NMR for the study of chain dynamics and structural constraints in polymeric soft materials, Prog Nucl Mag Res Sp 51 (2007) 1–35.
[41] M. Iza, S. Woerly, C. Danumah, S. Kaliaguine, M. Bousmina, Determination of pore size distribution for mesoporous materials and polymeric gels by means of DSC measurements: thermoporometry, Polymer 41 (2000) 5885–5893.
[42] P.D. Hong, J.H. Chen, Network structure and chain mobility of freeze-dried polyvinyl chloride dioxane gels, Polymer 39 (1998) 5809–5817.
[43] X.B. Hu, M. Vatankhah-Varnoosfaderani, J. Zhou, Q.X. Li, S.S. Sheiko, Weak hydrogen bonding enables hard, strong, tough, and elastic hydrogels, Adv. Mater. 27 (2015) 6899–6907.
[44] S.J. Lee, S.S. Kim, Y.M. Lee, Interpenetrating polymer network hydrogels based on

poly(ethylene glycol) macromer and chitosan, Carbohyd Polym 41 (2000) 197–205.
[45] T. Canal, N.A. Peppas, Correlation between mesh size and equilibrium degree of swelling of polymeric networks, J. Biomed. Mater. Res. 23 (1989) 1183–1193.
[46] Y. Chen, Y.H. Zhang, L.J. Zhao, ATR-FTIR spectroscopic studies on aqueous LiClO4, NaClO4, and mg(ClO4)(2) solutions, Phys. Chem. Chem. Phys. 6 (2004) 537–542.
[47] K. Nakamura, T. Hatakeyama, H. Hatakeyama, Relationship between hydrogen-bonding and bound water in Polyhydroxystyrene derivatives, Polymer 24 (1983) 871–876.
[48] K.F. Zieminski, N.A. Peppas, Diluent diffusion in polymer-diluent systems near Tg - migration of phthalic esters from Pvc to water, J. Appl. Polym. Sci. 28 (1983) 1751–1765.
[49] A.R.S. Couto, A. Ryzhakov, T. Loftsson, Disruption of alpha- and gamma-cyclodextrin aggregates promoted by chaotropic agent (urea), J Drug Deliv Sci Tec 48 (2018) 209–214.
[50] G. Hoch, A. Chauhan, C.J. Radke, Permeability and diffusivity for water transport through hydrogel membranes, J Membrane Sci 214 (2003) 199–209.
[51] G.M. Cruise, D.S. Scharp, J.A. Hubbell, Characterization of permeability and network structure of interfacially photopolymerized poly(ethylene glycol) diacrylate hydrogels, Biomaterials 19 (1998) 1287–1294.
[52] N.A. Peppas, H.J. Moynihan, L.M. Lucht, The structure of highly crosslinked poly(2-hydroxyethyl methacrylate) hydrogels, J. Biomed. Mater. Res. 19 (1985) 397–411.
[53] R. Stadler, L.D. Freitas, Thermoplastic elastomers by hydrogen-bonding.1. Rheological properties of modified polybutadiene, Colloid Polym. Sci. 264 (1986) 773–778.
[54] L. Bistricic, G. Baranovic, M. Leskovac, E.G. Bajsic, Hydrogen bonding and mechanical properties of thin films of polyether-based polyurethane-silica nanocomposites, Eur. Polym. J. 46 (2010) 1975–1987.
[55] L. Masaro, X.X. Zhu, Physical models of diffusion for polymer solutions, gels and solids, Prog. Polym. Sci. 24 (1999) 731–775.
[56] J.Q. Lai, Z. Li, Y.H. Lu, Z. Yang, Specific ion effects of ionic liquids on enzyme activity and stability, Green Chem. 13 (2011) 1860–1868.
[57] S.R. Lustig, N.A. Peppas, Solute diffusion in swollen membranes.9. Scaling Laws for solute diffusion in gels, J. Appl. Polym. Sci. 36 (1988) 735–747.
[58] N.A. Peppas, C.T. Reinhart, Solute diffusion in swollen membranes.1. A new theory, J Membrane Sci 15 (1983) 275–287.
[59] B. Amsden, Solute diffusion within hydrogels. Mechanisms and models, Macromolecules 31 (1998) 8382–8395.
[60] R.I. Cukier, Diffusion of Brownian spheres in semidilute polymer solutions, Macromolecules 17 (1984) 252–255.
[61] A. Vonjena, H.E. Lessing, Rotational-diffusion anomalies in dye solutions from transient-dichroism experiments, Chem. Phys. 40 (1979) 245–256.
[62] G.E. Zajkov, Chemical and Biochemical Kinetics Mechanism of Reactions, Nova Science Publishers, New York, 2004.
[63] P.J.M. Stals, M.A.J. Gillissen, R. Nicolaÿ, A.R.A. Palmans, E.W. Meijer, The balance between intramolecular hydrogen bonding, polymer solubility and rigidity in single-chain polymeric nanoparticles, Polym Chem-Uk 4 (2013) 2584–2597.
[64] L. Hou, F. Lanni, K. Lubyphelps, Tracer diffusion in F-actin and Ficoll mixtures - toward a model for cytoplasm, Biophys. J. 58 (1990) 31–43.
[65] E. De Rosa, F. Urciuolo, C. Borselli, D. Gerbasio, G. Imparato, P.A. Netti, Time and space evolution of transport properties in agarose-chondrocyte constructs, Tissue Eng. 12 (2006) 2193–2201.